Journal of Biomechanics 88 (2019) 88–94

Contents lists available at ScienceDirect

Journal of Biomechanics

journal homepage: www.elsevier.com/locate/jbiomech
www.JBiomech.com

In vitro analysis of blood flow in a microvascular network with realistic geometry

Yuya Kodama [a,b], Hiroyoshi Aoki [b], Yutaka Yamagata [b], K. Tsubota [a,b,*]

[a] Graduate School of Engineering, Chiba University, 1-33 Yayoi, Inage, Chiba 263-8522, Japan
[b] RIKEN Center for Advanced Photonics, RIKEN, 2-1 Hirosawa, Wako, Saitama 351-0198, Japan

ARTICLE INFO

Article history:
Accepted 14 March 2019

Keywords:
Biomechanics
Microcirculation
Blood flow
Red blood cells
Hematocrit
Micro channel

ABSTRACT

In vitro blood flow was measured in a polydimethysiloxane micro channel to reflect the complex geometry of a microvascular network. Flow rates were determined from the velocities of tracer particles moving along the center line of the flow channel, and the flow rates of two working fluids were then compared: water and blood. In some bifurcating channels, the measured flow rate showed that the effects of bifurcation in the apparent viscosity depend on the hematocrit, such that the flow rate in the daughter channel with the higher (lower) flow rate was lower (higher) for blood than for water. The measured flow rates in other bifurcating channels reflected effects from the surrounding flow channels acting as bypasses, which tended to balance out the effects of bifurcation.

1. Introduction

The mechanics of blood flow in microcirculation have been studied for many years (Lipowsky, 2005; Pries et al., 1996a). The physical properties of blood when it acts as a working fluid have important effects on the flow behavior. These properties are typically represented in terms of the apparent viscosity, as a function of a hematocrit, and the viscoelastic properties of individual red blood cells. Another factor is the geometry of the microvascular network that serves as the flow channel, which is characterized in terms of the lengths and cross-sectional areas of individual vessels as well as their connectivity. The present study addresses on how the geometry of a microvascular network influences blood flow.

In vivo experiments have suggested that blood-flow behavior in microcirculation is associated with the geometry of microvessels. For example, the hematocrit distribution and pressure drop are affected by the geometry of microvessels and the network structure (Pries et al., 1996b). Additionally, the flow rate tends to decrease as the diameter of the blood vessels decreases (Kloosterman et al., 2014; Maibier et al., 2016). However, the effects of the microvascular network structure on blood flow remain unclear.

Previous *in vivo* studies have shown the challenges involved in identifying the correct geometry of microvessels with experiments aimed at measuring blood flow in intact tissue (Cokelet et al., 1998; Pries et al., 1994). The *in vitro* experiment discussed below has enabled us to use channels with an ideal geometry and, therefore, is appropriate for quantitative clarification of the relationship between blood flow and the geometry of microvessels. Previously reported *in vitro* experiments have evaluated the properties of blood flow including the axial concentration of red blood cells and the plasma layer near the channel wall in a straight tube (Goldsmith et al., 1989) and the characteristic motions of red blood cells in a bifurcating tube (Clavica et al., 2016; Hu et al., 2015; Leble et al., 2011; Shen et al., 2016).

The vessel of microvascular networks has a complex geometry. It is curved rather than straight, with changing cross-sectional geometry, and it may bifurcate and then merge to create multiple flow paths. All of these aspects have an effect on the blood flow (Balogh and Bagchi, 2017). Additionally, the structural characteristics may affect the blood flow patterns because of the motion of blood cells (Gould and Linninger, 2015), which in turn determine the hematocrit distribution (Stauber et al., 2017).

In vitro experiments reported to date have not investigated physiologically realistic vessel geometries. To overcome this limitation, the present study used a polydimethysiloxane (PDMS) flow channel that was fabricated to evaluate the complex geometry of microvascular networks in two dimensions. The flow rate through the PDMS channel was measured using two working fluids, pure water and stored rabbit blood. The flow rates were calculated by

* Corresponding author at: Graduate School of Engineering, Chiba University, 1-33 Yayoi, Inage, Chiba 263-8522, Japan.
E-mail address: tsubota@faculty.chiba-u.jp (K. Tsubota).

https://doi.org/10.1016/j.jbiomech.2019.03.022
0021-9290/

measuring the velocities of tracer particles along the center line of the flow channel, and multiplying these velocities by the cross-sectional area of the channel. These measurements allow us to evaluate the difference in the flow rates of water and blood. Using the flow rate measurements, we show how both the bypass and hematocrit distribution following Zweifach-Fung bifurcation effects (Li et al., 2012) determine the flow of blood in a channel network.

2. Methods

2.1. Micro flow channel

Using the soft lithographic technique (Lima et al., 2008), a PDMS micro flow channel with rectangular cross section was fabricated, as shown in Fig. 1(a). The PDMS micro flow channel was built with reference to the microvascular network of the rabbit omentum that was used for *in vivo* blood flow measurements (Zweifach and Lipowsky, 1977). The flow channel has a complex microvascular geometry characterized by two-dimensional curved centerlines, the distribution of cross-sectional areas, and the connectivity of vessels. One inlet and outlet were present in the channel. The widths of the channel ranged from 5 to 23 μm. The total length along the centerlines was 2946 μm. Briefly, the two-dimensional channel geometry was constructed manually using CAD software (Jw_cad, http://www.jwcad.net/). This geometry was subsequently printed on a photomask from Toyo Precision Parts Mfg. (Nara, Japan) and transferred to a spin-coated SU-8 3050 (Nippon Kayaku, Co., Ltd, Tokyo, Japan) on a silicon wafer. After the channel geometry pattern was cross-linked by baking, the SU-8 substrate, except for the pattern, was dissolved using 2-methoxy-1-methylethyl acetate (PGMEA, Wako, Tokyo, Japan). Consequently, the SU-8 channel mold was obtained. PDMS (Sylgard 184, Dow Corning Toray Co., Ltd., Tokyo, Japan) was then poured in the mold and baked at 75 °C for 1 h. The PDMS channel was then peeled from the mold and sealed firmly using a coverslip. An optical surface profiler (NewView™ 7200, Zygo, CT, USA) was used to measure the thickness of the SU-8 channel mold, and the mold was approximately 10.4–10.6 μm thick. The average thickness of H = 10.5 μm was considered as the depth of the PDMS flow channel.

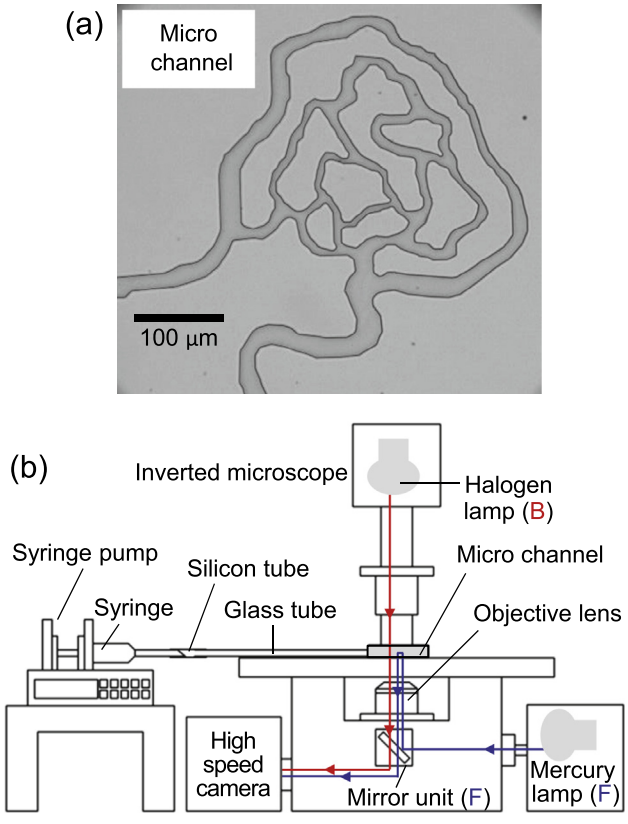

Fig. 1. Experimental apparatus for flow measurement in micro channel. (a) PDMS micro channel as a model of a microvascular network. (b) Perfusion and observation devices. Lines with arrowheads indicate the optical paths of fluorescent observations (blue, F) of tracers in water, and of bright field observations (red, B) of red blood cells in blood. (For interpretation of the references to color in this figure legend, the reader is referred to the web version of this article.)

2.2. Working fluids

Stored rabbit blood (Kohjin Bio, Saitama, Japan) and pure water (FUJIFILM Wako Pure Chemical Corporation, Osaka, Japan) were tested as working fluids. To prevent coagulation, the blood sample was adjusted to include 2 mM ethylenediaminetetraacetic acid (EDTA) (Dojindo Molecular Technologies, Tokyo, Japan). After the stored rabbit blood was centrifuged at 1500*g* for 5 min, the supernatant was removed and the red blood cells were suspended with one volume of Alsever's solution (Nippon Bio-Test Laboratories, Saitama, Japan). This process was repeated three times. Filter paper (No. 1, Advantec Toyo, Tokyo, Japan) was subsequently used to remove all cell aggregates present in the blood; this blood was then centrifuged at 1500*g* for 5 min, and the red blood cells were mixed with two volumes of Alsever's solution. Finally, the blood sample was re-adjusted to include 2 mM EDTA. Hematocrit (Ht) in the stationary state was measured as 27% after centrifuging the blood in a 100-μm-diameter glass tube at 2300*g* for 30 min. In the pure water working fluid, fluorescent particles with 1-μm diameters (FluoSpheres® carboxylate, Cat. F8823, Life Technologies, CA, USA) were suspended at 7.3×10^7/ml. The red blood cells and fluorescent particles were used as tracer particles for visualizing the flows.

2.3. Experimental setup

Fig. 1(b) shows a schematic drawing of the perfusion device we used. A 1-ml syringe (SS-01T, TERUMO, Tokyo, Japan) containing the working fluid was connected to the PDMS micro channel via a glass tube with diameter of 0.13 mm and length of 120 mm (Fujirika-Kougyou, Osaka, Japan) and a silicone tube with length of approximately 10 mm. The flow was driven by a syringe pump (KDS 210, Kd Scientific, MA, USA). The pumping speed was constant and was set to create a flow rate of 1.67×10^{-12} m^3/s at the syringe. The test section of the PDMS micro channel, corresponding to a modeled microvascular channel network (Fig. 1), was positioned on the stage of an inverted microscope (IX71, Olympus, Tokyo, Japan). To observe the moving tracer particles, a series of microscope images were recorded using a high-speed camera (FASTCAM Mini AX100, Photron, Tokyo, Japan) through a dry 40× objective lens with a numerical aperture of 0.75. The resolution of the recorded data was 1 μm/pixel in space and 4000 frame/s in time. The focus of the microscope was fixed at the middle of the micro channel in the depth direction. Fluorescent observations were performed for fluorescent tracer particles in water. A mirror unit (U-MNIBA3, Olympus, Tokyo, Japan) with optical filters for excitation (470–495 nm) and absorption (510–550 nm) was used with a high-pressure Mercury lamp (U-HGLGPS, Olympus, Tokyo, Japan) as the light source. Bright field observations were performed to measure the red blood cells in the blood, using a Halogen lamp (7724, Philips, Amsterdam, Netherlands) as the light source.

2.4. Flow rate measurement

Series of microscope images of the tracer particles were recorded for both water and blood. The observations are reported

in videos that can be found in the supplementary materials and the snapshots shown in Fig. 2. To quantify the flow rate using the recorded microscope images, the entire flow channel was divided into 32 segments. They are marked by A to V and Z1 to Z10 in Fig. 3. The channel segments were mostly set between two neighboring junctions. Long channels between neighboring junctions were further divided into several segments, such as (A, Z1), (B, Z2, Z3, U), (N, Z4), (P, Z7), and (V, Z10), to consider the hematocrit distribution and give better estimates of flow resistance (see Section 2.5). A single point for flow rate measurement was set in each of the 22 channel segments A to V. For these measurement points, the velocities of the tracer particles were determined from the microscope images as follows. For the microscope image at time t, the tracer particle nearest the measurement point and along the centerline of the flow channel was carefully selected. The position $\boldsymbol{x}(t)$ of the centroid of the tracer particle was manually determined using a mouse pointer on the microscope image (lower parts of Fig. 2). The same procedure was performed for the neighboring frame at time $t+\Delta t$ to determine the position $\boldsymbol{x}(t+\Delta t)$ of the same tracer particle. Finally, the velocity of the tracer particle was determined as $v=\Delta x/\Delta t$, with the tracer displacement as $\Delta x=|\boldsymbol{x}(t+\Delta t)-\boldsymbol{x}(t)|$. This measurement was applied for all tracer particles that were chosen for velocity measurements. When making the position $\boldsymbol{x}$ of the tracer particle with a mouse pointer, image recording software (PFV, Photron, Japan) was used. The pixel size of the images was 1 μm. The flow rate Q was then determined as

$$Q = CHW_{\mathrm{P}}v \tag{1}$$

assuming that the velocity v of the tracer particle was the flow velocity at the centerline of the channel. In Eq. (1), H is the channel height (Section 2.1), W_{P} is the channel width at the measurement points, and C is the ratio of mean velocity U_{mean} to the maximum $U_{\max}$ in a rectangular channel with aspect ratio $A_{\mathrm{P}}=W_{\mathrm{P}}/H$ at the cross section (Lima et al., 2006) as

$$C=\frac{U_{\mathrm{mean}}}{U_{\max}}=\frac{\pi^3}{48}\frac{\left[1-\sum_{n,odd}^{\infty}\frac{192}{n^5\pi^5A_{\mathrm{P}}}\tanh\left(n\pi\frac{A_{\mathrm{P}}}{2}\right)\right]}{\sum_{n,odd}^{\infty}\frac{1}{n^3}\left[1-\frac{1}{\cosh\left(n\pi\frac{A_{\mathrm{P}}}{2}\right)}\right]\sin(n\frac{\pi}{2})}. \tag{2}$$

This value ranges from 0.47 – 0.52 in our flow channel. The calculation of Q in Eq. (1) was performed for 10 tracer particles for each

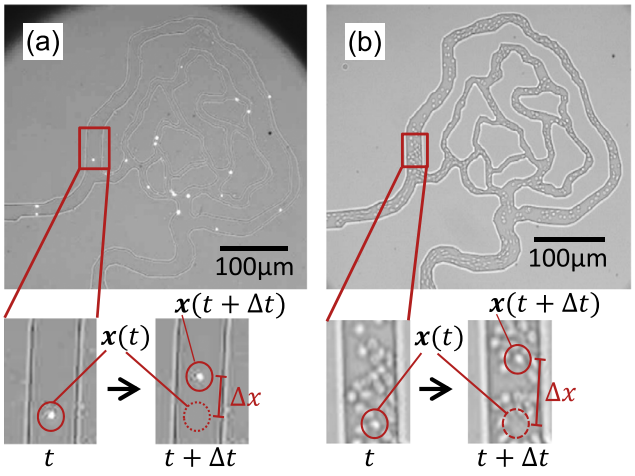

Fig. 2. Snapshots of tracer particles acquired in experiments with (a) water and (b) blood. The lower part shows the tracer displacement $\Delta x=|\boldsymbol{x}(t+\Delta t)-\boldsymbol{x}(t)|$ determined from two neighboring frames to obtain velocity $v=\Delta x/\Delta t$. The number of red blood cells (RBCs) is counted to determine the hematocrit of the blood. For example, $N=22$ RBCs were counted in the lower right of (b).

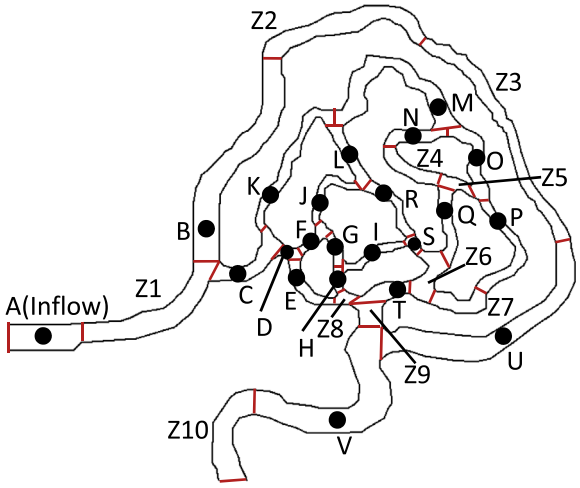

Fig. 3. Thirty-two channel segments (A to V and Z1 to Z10) in which hematocrit was measured. A point for measuring flow rates was determined in each of the 22 channel segments (A to V).

measurement point, and the mean and standard deviation of Q were determined.

In order to avoid fluctuations in the measured velocity v caused by small deviations of the tracer position from the centerline, the positions of measurement points A to V were selected to be at parts of the channels that were straight and of constant width (Fig. 3). Flow rates were not measured at Z1 to Z10; velocity measurements at segments Z5, Z6, Z8 and Z9 were difficult due to the short length of the segment. Because the flow rate Z1 was essentially the same as that at the inflow (A), velocity measurements were omitted for Z1; similarly, it was also omitted for Z2 and Z3 (the same with B), Z4 (N), Z7 (P) and Z10 (V). In our experimental setup, the inlet flow velocity fluctuated on the time scale of ten seconds, although it was stable on the time scale of milliseconds (Supplementary materials). This flow fluctuation was likely due to elastic deformation of the syringe pump and silicon tube used in the experimental setup. Therefore, the visually-stable flow state was selected for the velocity measurements.

2.5. Fluid analysis and hematocrit measurement

Fluid analysis was performed to clarify the measured flow rate distribution using an electric circuit model (Lipowsky and Zweifach, 1974) constructed from the geometries and connectivity of 32 channel segments marked in Fig. 3. Briefly, the flow resistance R of each flow channel segment was determined as

$$R=\frac{12\mu L}{H^3W_{\mathrm{S}}}\frac{1}{1-\sum_{n,odd}^{\infty}\frac{192}{n^5\pi^5A_{\mathrm{S}}}\tanh\left(n\pi\frac{A_{\mathrm{S}}}{2}\right)}, \tag{3}$$

assuming a straight rectangular channel. In Eq. (3), W_{S} is the mean width of the channel segment, and L is the length along the centerline; these values are summarized in Table 1 for segments that involve measurement points of the flow rate. $A_{\mathrm{S}}=W_{\mathrm{S}}/H$ is the aspect ratio of the channel segment. While constant viscosity $\mu=\mu_0=1$ mPa · s was set for the water, the apparent viscosity $\mu=\mu_{\mathrm{blood}}$ of the blood was assumed to follow a simple increasing function of the instantaneous hematocrit Ht [%] (Charm and Kurland, 1972) as

$$\mu_{\mathrm{blood}}=\frac{\mu_0}{1-\alpha\frac{Ht}{100}}. \tag{4}$$

In Eq. (4), α, a constant according to the cross-sectional geometry of the flow channel, was set to 2 in this study. Using the continuity equation in terms of the flow rate at the junction of channel

Table 1
Widths and lengths of channel segments illustrated in Fig. 3.

Segment	A	B	C	D	E	F	G	H	I	J	K
W_s [μm]	23	22	13	10	10	8	9	8	5	7	10
L [μm]	97	196	72	23	75	33	42	29	77	86	157

Segment	L	M	N	O	P	Q	R	S	T	U	V
W_s [μm]	9	12	11	11	6	12	8	8	12	18	22
L [μm]	66	168	62	77	120	75	74	29	50	239	178

Segment	Z1	Z2	Z3	Z4	Z5	Z6	Z7	Z8	Z9	Z10
W_s [μm]	20	15	11	12	8	8	12	10	22	23
L [μm]	139	162	245	62	34	33	72	26	28	120

segments and the equilibrium equations at a channel segment, a set of linear equations $[1/R]\{P\} = \{dQ\}$ was constructed and $\{P\}$ was computed. Here $[1/R]$ is the matrix of flow conductance, and $\{P\}$ and $\{dQ\}$ are the pressure and difference in the flow rate between inward and outward flows, respectively, at the points corresponding to the inlet, outlet, and junctions of the channel segments (Lipowsky and Zweifach, 1974).

RBCs of various sizes and shapes have been observed in rabbit blood (Mitruka and Rawnsley, 1981). In our bright-field microscope observation, diameters of RBCs ranged from approximately 4–6 μm, and RBCs appeared to have biconcave disk or spherical shapes. Thus, when calculating *Ht*, a red blood cell was assumed to have a biconcave disk shape similar to that of human (Evans and Fung, 1972) with diameter $d = 5$ μm, maximum thickness $t = 1.65$ μm, and volume $V = 24.6$ μm^3. In addition, assuming that a single red blood cell occupies a $d \times d \times t$ cuboid region, the local volume fraction of the red blood cell in the cuboid was calculated as $\phi = V/(d^2 t) = 0.60$. Furthermore, with the small thickness of the micro channel, the red blood cell in the channel was further assumed to be positioned such that the normal direction of the disk plane of the cell was directed in the thickness direction of the channel. With these assumptions, the number N of red blood cells existing around the center plane in the depth direction (i.e., the focus plane of the microscope) was counted carefully [Fig. 2 (b)], and the hematocrit value for the thin region involving the focus plane with thickness t was determined as $Ht^C = N(\phi d^2 t)/(LW_S t) = N\phi d^2/(LW_S)$. Finally, assuming a uniform distribution of red blood cells in the thickness direction, Ht^C was regarded as *Ht* of a channel segment. This *Ht* calculation was performed for five frames of each channel segment, and the mean and standard deviation were determined.

3. Results

3.1. Measurements of flow rate and hematocrit

Fig. 4 shows the measured flow rates in the micro channel. The flow rates at measurement point A (Inflow) were $1.94 \pm 0.16 \times 10^{-12}$ m^3/s (mean ± s.d.) for pure water and $2.22 \pm 0.17 \times 10^{-12}$ m^3/s for blood. The mean flow rate was higher by 16–33% compared to the flow rate set at the syringe pump (Section 2.3). This observation is likely to be related to the sampling points at which a flow was judged to be stable. The flow rate diminished as the flow channel bifurcated. The minimum flow rate was measured at I ($0.04 \pm 0.006 \times 10^{-12}$ m^3/s for water and $0.06 \pm 0.01 \times 10^{-12}$ m^3/s for blood). In contrast, the flow rate was higher at the flow paths through the inside of the micro channel (e.g., flow paths: CK, CDE, and CDF) relative to that on its outside (e.g., flow path: BU). These findings are illustrated by the flow rates of B and C in Fig. 4. When the working fluid was blood, the measured mean hematocrit *Ht* ranged between 0% and 20%, as

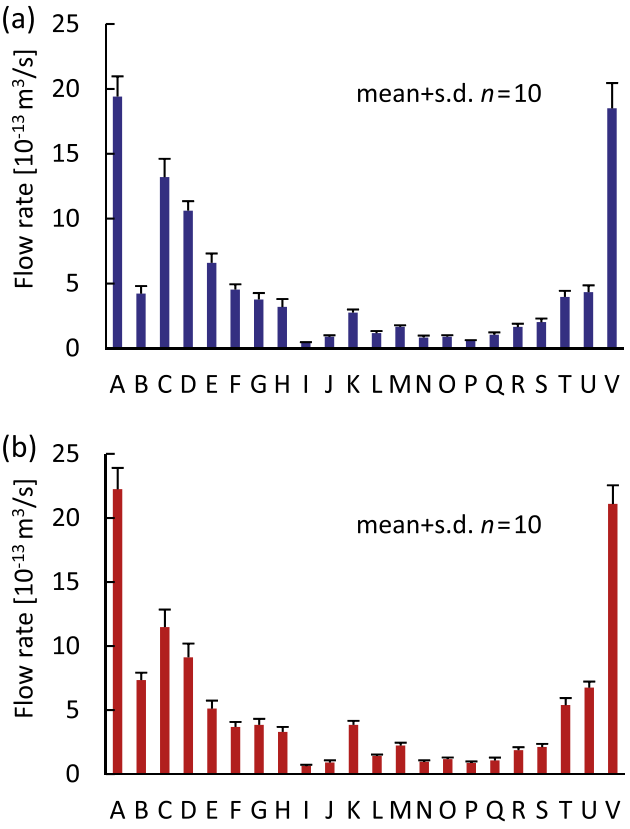

Fig. 4. Measured flow rate at 22 measurement points for (a) water and (b) blood.

shown in Fig. 5. The standard deviation of *Ht*, ranging between 0% (J) and 7.0% (Z8), increased with decreasing length of the flow channel segment.

To compare the flow of the two working fluids, the measured flow rates were normalized by those at the inflow (measurement point A). This data is given as blue (water) and red (blood) colored bars in Fig. 6. For the measurement points B, I, K, L, M, N, O, P, T and U, the normalized flow rate was higher for blood than for water. On the contrary, the normalized flow rate was lower for the other points. The magnitude relationship of the normalized flow rate between working fluids is consistent with our fluid analysis results (illustrated by hatched bars in Fig. 6) at 17 measurement points, except for Q, R, and S. These results support the finding that the measured flow rates reflect the difference in the flow behaviors of the two working fluids.

3.2. Effects of bifurcation and bypass on flow rate distribution

In the two daughter blood vessels that branch from a parent blood vessel, the daughter blood vessel with a higher (lower) flow

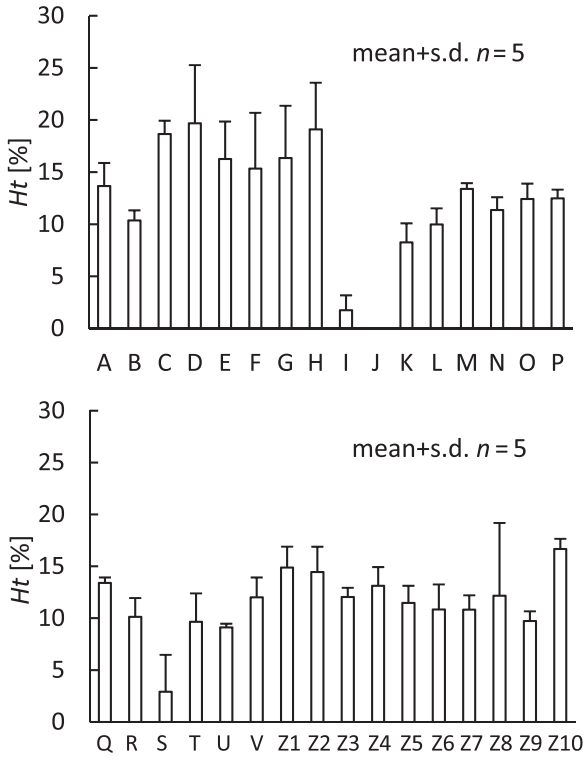

Fig. 5. Measured hematocrit at 32 measurement segments.

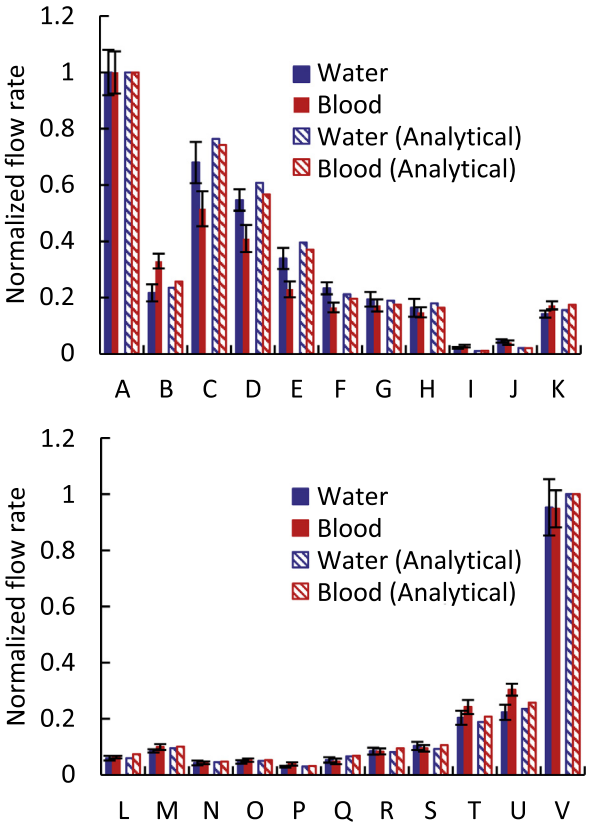

Fig. 6. Flow rates normalized by the flow rate at the inflow (measurement point A) for the experimental measurements (filled bars) and fluid analysis using an electric circuit model (hatched bars). For both filled and hatched bars, blue (left) and red (right) indicate water and blood, respectively. (For interpretation of the references to color in this figure legend, the reader is referred to the web version of this article.)

Table 2
Flow rate ratio and hematocrit at 7 pairs of two daughter vessels. The major effect on the flow rate ratio is also listed as bifurcation, bypass, or bifurcation nearly equaling bypass.

Daughter channels	Flow rate ratio		Hematocrit [%]	Major effects
	Water	Blood		
C & B	76:24	61:39	19 & 10	Bifurcation
D & K	79:21	70:30	20 & 8	Bifurcation
E & F	59:41	58:42	16 & 15	Bifurcation
G & J	81:19	81:19	16 & 0	Bifurcation ≅ Bypass
H & I	88:12	84:16	19 & 2	Bifurcation
M & L	59:41	61:39	13 & 10	Bypass
O & N	52:48	55:45	12 & 11	Bypass

rate relative to the other daughter blood vessels has a higher (lower) hematocrit with more (less) red blood cells. These observations are known as the Zweifach–Fung effect (Li et al., 2012). In the daughter channel with the high (low) flow rate, this effect is likely to cause a decrease (increase) in the flow rate, along with an increase (decrease) in the apparent viscosity. As shown in Table 2 and Fig. 7, we observed this behavior at four of seven bifurcations. For example, the high flow rate at C relative to B determined the high apparent viscosity following to the high hematocrit. As a consequence, the difference in flow rate at C relative to B of blood (61:39) was lower than that of water (76:24). This phenomenon is also explained by the pressure drops along two flow paths, termed "α" and "β," neighboring C and B, as illustrated in Fig. 8(a). The pressure was obtained by a fluid analysis based on the electric circuit model. This pressure data was then normalized to be unity at the common starting point (marked "3" in Fig. 8(a)) and zero at the common ending point (marked "7"). The pressure drop along path α did not differ much between water and blood. This demonstrates that in the pressure drop, the increasing effects of high hematocrit were balanced with the decreasing effects of low flow rate. Along path β, the pressure drop at segments C and D was greater for blood than water; the increasing effects of the high flow rate on pressure drop were superior to the decreasing effects of the low hematocrit. The bifurcation effect tends to occur at high-flow-rate bifurcation sites (B and C, K and D, E and F, I and H), as illustrated in Fig. 7.

However, the above-described bifurcation effects do not explain the other three bifurcations. For example, the ratio of the flow rate between daughter channels G and J was the same (81:19) for both water and blood, even though both flow rate and hematocrit were higher at G than at J. A possible explanation for this finding is the decrease in pressure along the two flow paths, termed "α" and "β," neighboring G and J, as illustrated in Fig. 8(b). Here, the pressure was normalized to be unity at the common starting point (marked "8" in Fig. 8(b)) and zero at the common ending point (marked "14"). While the pressure drop along path α did not differ much between water and blood, the pressure drop along path β at segments D and F was greater for blood than water; this effect is due to the high hematocrit levels caused by the high flow rate at D relative to K (note that D and K are the two daughter channels from parent C). Following these pressure drops in the surrounding channels, the pressure drop in segment J was smaller for blood than for water. This effect nullified the bifurcation effects described above. Consequently, the flow rate distribution at the bifurcation form channels F to J and G was affected by the surrounding channels, where the flow path from K to L functioned as a bypass that affected the downstream pressure in segment J. The bypass effect tends to occur at sites with low rate (J and G, L and M, N and O), as illustrated by the blue color in Fig. 7.

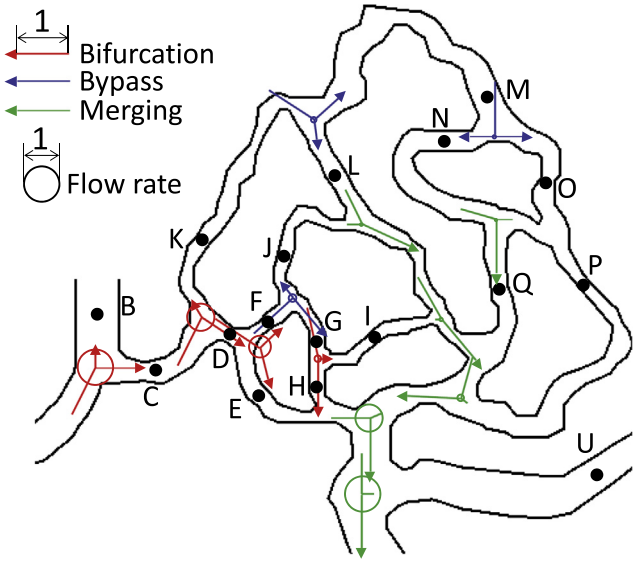

Fig. 7. Location of bifurcation effects (red) and bypass effects (blue). Merging sites are also marked (green). Arrow lines indicates flow direction (arrow heads) and the ratio of the flow rates between inward and outward flows at a junction (line lengths). The diameters of circles at junctions indicate the magnitude of flow rate relative to the flow rate at the inflow (A). (For interpretation of the references to color in this figure legend, the reader is referred to the web version of this article.)

The flow rates in low-flow-rate channels were generally higher in blood rather than water (e.g., by 31% at I, 32% at P, and 14% at O; Fig. 6). On the contrary, the flow rates in high-flow-rate channels were lower in blood than water (e.g., by 24% at C, 25% at D, and 32% at E; Fig. 6). This demonstrates that the red blood cells suspended in blood help make the flow distribution more uniform; these findings are consistent with those from *in vitro* experiments with asymmetric branching channels (Clavica et al., 2016) and numerical simulations (Wang et al., 2016).

4. Discussion

In this study, a micro PDMS rectangular flow channel was fabricated. The flow rate and hematocrit were measured in this channel using stored rabbit blood and pure water as the working fluids. The difference in the measured flow rate between the working fluids was mostly consistent with analytical results based on fluid mechanics, as shown in Fig. 6. This demonstrates that a micro channel with complex geometry was successfully fabricated.

The present study has certain limitations. First, as shown in Fig. 5, a large standard deviation was observed in the hematocrit measurements, particularly at short channel segments. This may be due to the sensitivity of instantaneous hematocrit to the time course of changes in blood flow. Second, compared to previously published *in vivo* experiments (Zweifach and Lipowsky, 1977), while the measured flow rate at point B was in agreement within

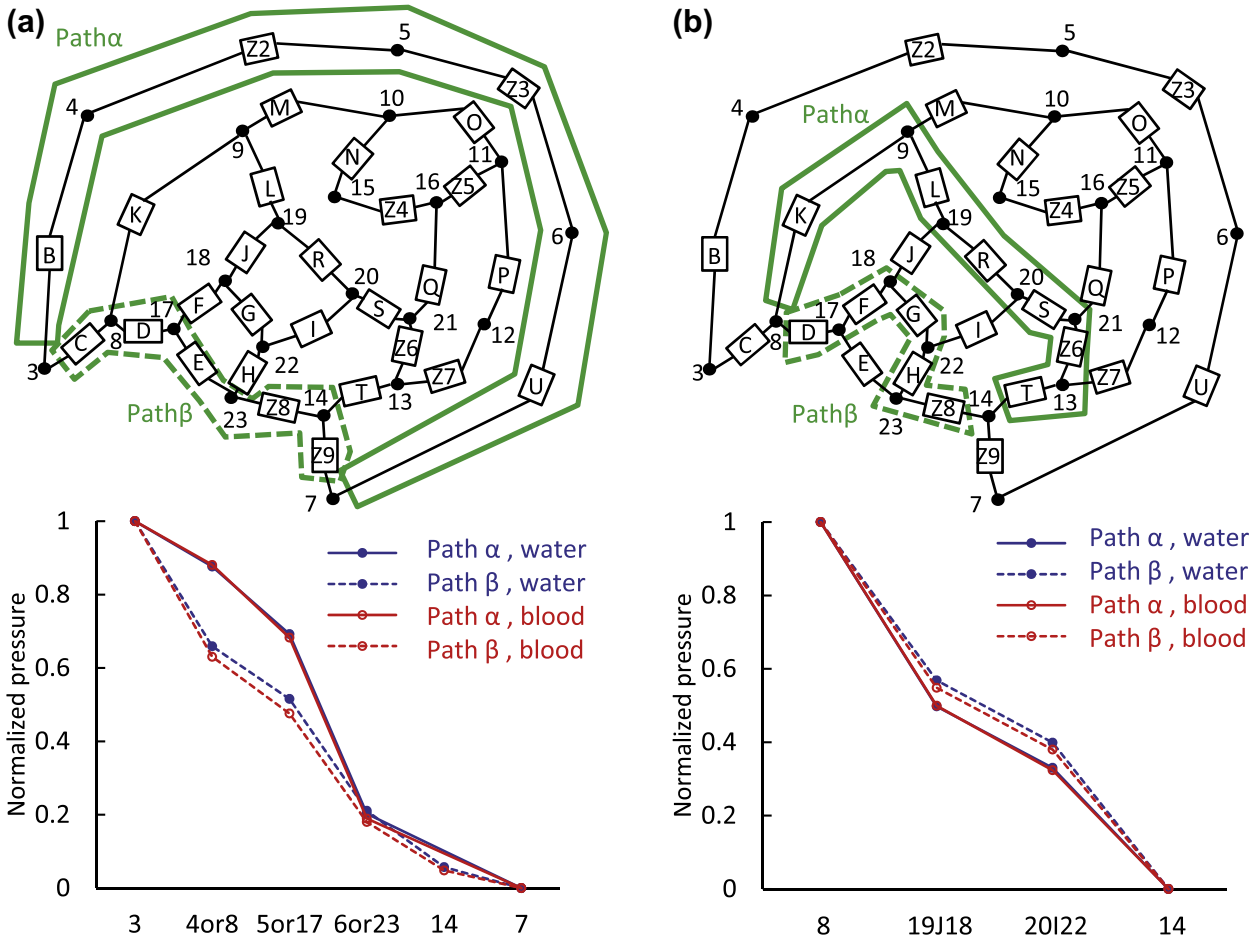

Fig. 8. Pressure drops along two flow paths neighboring bifurcations from Z1 to C and B (a) and from F to J and G (b). In (a), flow paths "α" (B–Z2–Z3–U) and "β" (C–D–E–Z8–Z9) have the same starting point "3" and ending point "7". In (b), flow paths "α" (K–L–R–S–Z6–T) and "β" (D–F–G–H–Z8) have the same starting point "8" and ending point "14". Pressure values were obtained by fluid analysis described in Section 2.5, and they were normalized and plotted as a function of channel location.

a 3% difference from the mean value, it differed by 92% at measurement point U, possibly because another existing flow channel that connects B and U was neglected. Third, the PDMS channel constructed in the present study is two-dimensional with constant depth, whereas the vessels in the above-mentioned *in vivo* experiments (Zweifach and Lipowsky, 1977) may differ in depth along the axial directions. These aspects are key points in developing *in vitro* experiments that more realistically represent a blood flow in intact tissues.

As stated in Section 3.1, the relationship between the magnitude of the normalized flow rates of water and blood was not completely consistent between the experimental data and fluid-mechanics analysis. In addition, the flow rates differ. At segment B for example, the flow rate of water was larger by 9% in the analytical results, while the flow rate of a blood was smaller by 12%. One of the reasons for this discrepancy is modeling errors in the fluid-mechanics analysis, such as the simplification of channel geometries. In addition, measurement errors in the tracer velocities are unavoidable, as some of the tracers used for measurements might not be sufficiently close to the centerline of the channel. In the case of blood, the measured hematocrit may have an error due to the distribution of red blood cells in the depth direction within a channel. The apparent viscosity determined by hematocrit (Eq. (4)) therefore may not be accurate due to the effects of the channel size. These effects might explain the difference between the analytical results and experimental data.

Rabbit red blood cells have smaller volume than a human red blood cells, and probably have different viscoelasticity. If a human blood were used in our experiment, the flow rate and pressure would be quantitatively different and would lead to change in the balance of effects of "bifurcation" and "bypass" on the blood flow. However, we believe that the difference between rabbit and human red blood cell will not change the conclusions of this study, such as the importance of two major effects of bifurcation and bypass, and the importance of pressure drops in understanding blood flow in a channel network.

Despite the above described limitations, our results demonstrate that the surrounding blood vessels function as a bypass and that Zweifach–Fung bifurcation effects (Li et al., 2012) determine the blood flow within a microvascular network. The bypass and bifurcation effects interact with each other. The results outlined in Table 2 indicate that both the bypass and bifurcation effects are important in the blood flow of a microcirculatory network. Further studies are needed, particularly about an intact microvascular network. Additionally, as shown in Fig. 8, we also find that the pressure drop is a good index for understanding the bypass effect in a channel network. This observation enhances our understanding of the currently available *in vivo* data, which mostly include measurements of flow velocity, flow rate and hematocrit (Pries et al., 1994).

Conflict of interest

The authors disclose no conflict of interest in relation to this publication.

Acknowledgments

This study was partly funded by a Grant-in-Aid for Scientific Research (15H03915), JSPS.

Appendix A. Supplementary material

Videos of flows of water (Suppl1.wmv) and blood (Suppl2.wmv) acquired during experimental sessions. Supplementary data to this article can be found online at https://doi.org/10.1016/j.jbiomech.2019.03.022.

References

Balogh, P., Bagchi, P., 2017. Direct numerical simulation of cellular-scale blood flow in 3D microvascular networks. Biophys. J . 113, 2815–2826.
Charm, S.E., Kurland, G.S., 1972. Blood Rheology. In: Bergel, D.H. (Ed.), Cardiovascular Fluid Dynamics. Academic Press, London and New York, pp. 157–203.
Clavica, F., Homsy, A., Jeandupeux, L., Obrist, D., 2016. Red blood cell phase separation in symmetric and asymmetric microchannel networks: effect of capillary dilation and inflow velocity. Sci. Rep. 6, 36763.
Cokelet, G.R., Pries, A.R., Kiani, M.F., 1998. Observations on the accuracy of photometric techniques used to measure some in vivo microvascular blood flow parameters. Microcirculation 5, 61–70.
Evans, E., Fung, Y.C., 1972. Improved measurements of the erythrocyte geometry. Microvasc. Res. 4, 335–347.
Goldsmith, H.L., Cokelet, G.R., Gaehtgens, P., 1989. Robin Fåhraeus: evolution of his concepts in cardiovascular physiology. Am. J. Physiol. 257, H1005–H1015.
Gould, I.G., Linninger, A.A., 2015. Hematocrit distribution and tissue oxygenation in large microcirculatory networks. Microcirculation 22, 1–18.
Hu, R., Li, F., Lv, J., He, Y., Lu, D., Yamada, T., Ono, N., 2015. Microfluidic analysis of pressure drop and flow behavior in hypertensive micro vessels. Biomed. Microdevices 17, 9959.
Kloosterman, A., Hierck, B., Westerweel, J., Poelma, C., 2014. Quantification of blood flow and topology in developing vascular networks. PLoS One 9, e96856.
Leble, V., Lima, R., Dias, R., Fernandes, C., Ishikawa, T., Imai, Y., Yamaguchi, T., 2011. Asymmetry of red blood cell motions in a microchannel with a diverging and converging bifurcation. Biomicrofluidics 5, 44120–4412015.
Li, X., Popel, A.S., Karniadakis, G.E., 2012. Blood-plasma separation in Y-shaped bifurcating microfluidic channels: a dissipative particle dynamics simulation study. Phys. Biol. 9, 026010.
Lima, R., Wada, S., Tanaka, S., Takeda, M., Ishikawa, T., Tsubota, K., Imai, Y., Yamaguchi, T., 2008. In vitro blood flow in a rectangular PDMS microchannel: experimental observations using a confocal micro-PIV system. Biomed. Microdev. 10, 153–167.
Lima, R., Wada, S., Tsubota, K., Yamaguchi, T., 2006. Confocal micro-PIV measurements of three-dimensional profiles of cell suspension flow in a square microchannel. Meas. Sci. Technol. 17, 797–808.
Lipowsky, H.H., 2005. Microvascular rheology and hemodynamics. Microcirculation 12, 5–15.
Lipowsky, H.H., Zweifach, B.W., 1974. Network analysis of microcirculation of cat mesentery. Microvasc. Res. 7, 73–83.
Maibier, M., Reglin, B., Nitzsche, B., Xiang, W., Rong, W.W., Hoffmann, B., Djonov, V., Secomb, T.W., Pries, A.R., 2016. Structure and hemodynamics of vascular networks in the chorioallantoic membrane of the chicken. Am. J. Physiol. – Heart Circulat. Physiol. 311, H913–H926.
Mitruka, B.M., and Rawnsley, H.M., 1981. Clinical Biochemical and Hematological Reference Values in Normal Experimental Animals and Normal Humans. 2nd ed. Masson Pub. USA.
Pries, A.R., Secomb, T.W., Gaehtgens, P., 1996a. Biophysical aspects of blood flow in the microvasculature. Cardiovasc. Res. 32, 654–667.
Pries, A.R., Secomb, T.W., Gaehtgens, P., 1996b. Relationship between structural and hemodynamic heterogeneity in microvascular networks. Am. J. Physiol. 270, H545–H553.
Pries, A.R., Secomb, T.W., Gessner, T., Sperandio, M.B., Gross, J.F., Gaehtgens, P., 1994. Resistance to blood flow in microvessels in vivo. Circ. Res. 75, 904–915.
Shen, Z., Coupier, G., Kaoui, B., Polack, B., Harting, J., Misbah, C., Podgorski, T., 2016. Inversion of hematocrit partition at microfluidic bifurcations. Microvasc. Res. 105, 40–46.
Stauber, H., Waisman, D., Korin, N., Sznitman, J., 2017. Red blood cell dynamics in biomimetic microfluidic networks of pulmonary alveolar capillaries. Biomicrofluidics 11, 014103.
Wang, T., Rongin, U., Xing, Z., 2016. A micro-scale simulation of red blood cell passage through symmetric and asymmetric bifurcated vessels. Sci. Rep. 6, 20262.
Zweifach, B.W., Lipowsky, H.H., 1977. Quantitative studies of microcirculatory structure and function. III. Microvascular hemodynamics of cat mesentery and rabbit omentum. Circ. Res. 41, 380–390.